THE JOURNAL OF PHYSICAL CHEMISTRY A

Article

pubs.acs.org/JPCA

Matrix Photochemical Study and Conformational Analysis of $CH_3C(O)NCS$ and $CF_3C(O)NCS$

Luis A. Ramos,[†] Sonia E. Ulic,[†] Rosana M. Romano,[†] Helmut Beckers,[‡] Helge Willner,[‡] and Carlos O. Della Védova*[,†]

[†]CEQUINOR (UNLP-CONICET), Departamento de Química, Facultad de Ciencias Exactas, Universidad Nacional de La Plata, 47 esq. 115, 1900 La Plata, República Argentina

[‡]Fachbereich C - Anorganische Chemie, Bergische Universität Wuppertal, 42097 Wuppertal, Germany

ABSTRACT: The vapor of acetyl isocyanide, $CH_3C(O)NCS$, and trifluoroacetyl isocyanide, $CF_3C(O)NCS$, were isolated in solid Ar at 15 K. The existence of rotational isomerism was confirmed when the matrixes were irradiated with broad-band UV−vis light ($200 \leq \lambda \leq 800$ nm) and also by temperature-dependent Ar-matrix IR spectroscopy. The initial spectra showed the vapor of $CH_3C(O)NCS$ and $CF_3C(O)NCS$ consist of two conformers syn−syn and syn−anti (with the C═O bond syn with respect to the C−H or C−F bond and syn or anti with respect to the N═C double bond). When $CH_3C(O)NCS$ is irradiated, simultaneously with the randomization process, H_2CCO and HSCN are produced. In the case of the photolysis of $CF_3C(O)NCS$, the main products are CF_3NCS and CO. The assignment of the IR bands to the different photoproducts was made on the basis of the usual criteria, taking account reported antecedents in the literature.

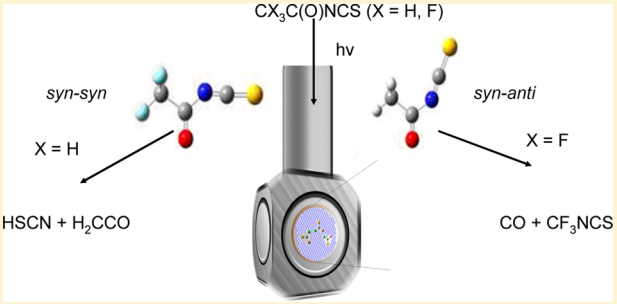

INTRODUCTION

Our research group in La Plata has been interested for some time in the matrix photochemistry of relatively small molecules. For example, $ClF_2CC(O)NCS$ has been recently shown to possess a rich photochemistry involving a variety of reaction pathways that we have wanted to elucidate.[1] Several studies on thio- and isothiocyanates compounds have been carried out in recent times related to their wide variety of medicinal, pharmaceutical, and industrial applications. They are also part of cruciferous vegetables. Their use in the daily diet appears to be associated with a reduced risk of degenerative diseases. Their valuable spectroscopic and electronic properties in ground and excited states have been also reported.[2−5] Vibrational chromophores that are sensitive to local electrostatic environment are useful probes of structural variations of proteins on subnanosecond time scales, but their short vibrational lifetimes may limit their applicability. The increase of the lifetime of nitrile probes by introducing heavy atoms between the probe and protein side chains has been recently reported. Stereoisomers of thiocyanato- and selenocyanato-derivatized prolines, Pro-SCN and Pro-SeCN, were synthesized, and their CN stretching lifetimes in D_2O and chloroform were measured with polarization-controlled IR pump−probe spectroscopy.[6]

The isothiocyanate species results energetically favored against its isomer thiocyanate. Using standard bond energies the bond breakage of a C−N═C═S fragment requires 1496 kJ/mol whereas this value reaches 1434 kJ/mol for the isomeric thiocyanante form, C−S−C≡N. The activation barrier between these two forms defines the kinetic of the isomerization. Therefore, the thiocyanate isomers may be elusive or almost difficult to isolate. This fact has been recently evidenced during the thiocyanomethylation of an intermediate in the synthesis of intervenolin, where the thiocyanate species spontaneously undergoes a pivotal rearrangement to the corresponding isothiocyanates isomer.[7,8] Some of these isomerization mechanisms have been studied, so it is the case of benzyl and alkyl (especially tert-butyl) thiocyanates, which rearrange via an ion pair mechanism in solution.[3,9−13] This chemistry, photochemistry, and their fundamental concepts can be also applied to understand interesting interstellar processes. For instance, the detection of thiocyanic acid, HSCN, has been recently reported[14] whereas its isomer isothiocyanic acid, HNCS, has been first identified in 1979 also in the giant molecular cloud, a stellar nursery made of gas and dust known as Sagittarius B2.[15] These outcomes must be related with their chemical nature and based on their electronic structures.

Therefore, in this work we will study two related isothiocyanates, acetyl- and trifluoroacetyl isothiocyanates, $CH_3C(O)NCS$ and $CF_3C(O)NCS$, combining photochemical, spectroscopic, and computation tools to obtain insights regarding the above-mentioned topics. The combination of a rigid, inert host, and low temperature enable the different conformers to be trapped and their thermal interconversion mostly quenched (kT at 15 K = 0.12 kJ mol^{-1}). Thus, no other

Received: November 8, 2013
Revised: December 19, 2013
Published: December 30, 2013

spectroscopic method combines the sensitivity of the matrix isolation technique with the structural information obtained when the support of computational chemistry is provided. In the present case, the interconversion of the conformers expected for both $CH_3C(O)NCS$ and $CF_3C(O)NCS$ can then be brought about by photolysis and thermal experiments. If the picture may be complicated by photoevolution or photodecomposition, this can also be exploited for the access to interesting and smaller photoproducts such as HSCN (from $CH_3C(O)NCS$) and CF_3NCS (from $CF_3C(O)NCS$). This fact invites also examination in connection with roaming mechanisms.[16] Roaming represents a mechanism implying a frustrated dissociation of a radical. This radical can experience large amplitude motions near the rest of its parent molecule retaining its association through van der Waals type attractions. Although this work does not present conclusive evidence for the existence of roaming in $CH_3C(O)NCS$ and $CF_3C(O)NCS$, the photoevolution channels of these species confirms that in principle such a mechanism is possible.

EXPERIMENTAL SECTION

Synthesis. Both $CH_3C(O)NCS$ and $CF_3C(O)NCS$ were synthesized by treatment of the corresponding acetyl or trifluoroacetyl chloride with an excess of silver thiocyanate, AgSCN, and subsequently characterized vibrationally.[17] For the preparation of $CH_3C(O)NCS$, 0.7 g of $CH_3C(O)Cl$ were distilled onto 1.5 g of dry AgSCN in a 250 mL glass vessel provided with a Young valve with PTFE stems (Young, London, U.K.). The reaction was carried out in vacuum for 0.5 h at −20 °C. Purification of the product was performed by trap-to-trap distillations with traps held at −15, −70, and −196 °C. $CH_3C(O)NCS$ was mainly isolated in the trap at −15 °C. The final yield was 90%. Silver thiocyanate was prepared from $AgNO_3$ and KSCN, and $CH_3C(O)Cl$ was formed by chlorination of the corresponding acid, $CH_3C(O)OH$, (Merck & Co.), with PCl_5.

The same scheme was used to prepare $CF_3C(O)NCS$. In this case, 0.5 g of $CF_3C(O)Cl$ and 0.9 g of AgSCN were used. The selected temperatures for the traps were −55, −92, and −196 °C. $CF_3C(O)NCS$ was isolated mainly in the first trap with a final yield of 80%. $CF_3C(O)Cl$ was obtained by chlorination of the corresponding acid, $CF_3C(O)OH$, (Merck & Co.), with PCl_5.

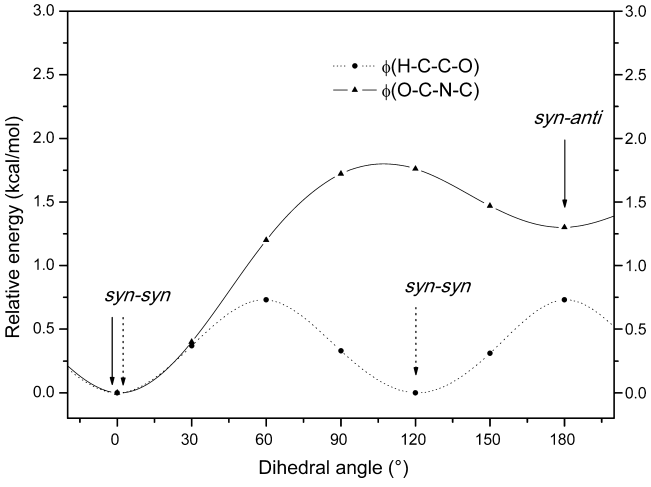

Figure 1. Potential energy curve of $CH_3C(O)NCS$ for rotation along C−C and C−N bonds calculated at B3LYP/6-311++(dp) level of approximation.

Instrumentation and Procedure. *(a). General Procedure.* Volatile materials were manipulated in a glass vacuum line equipped with a capacitance pressure gauge (221 AHS-1000, MKS Baratron, Burlington, MA), three U-traps and valves. The pure compounds were stored in flame-sealed glass ampules under liquid nitrogen in a Dewar vessel. The ampules were opened with an ampule key at the vacuum line, an appropriate amount was taken out for the experiments, and then they were flame-sealed again.[18] The vapor pressures of the samples were measured in a small vacuum line equipped with a calibrated capacitance pressure gauge (MKS Baratron, AHS-100) and a small sample reservoir. Both isothiocyanate compounds are liquid at ambient temperature.

(b). Vibrational Spectroscopy. Infrared gas spectra were recorded on a Bruker Vector 25 spectrometer and on a Bruker EQUINOX 55 FTIR spectrometer with a resolution of 2 cm^{-1} in the range from 4000 to 400 cm^{-1}.

Raman spectra of neat liquids were measured at room temperature in flame-sealed capillaries (3 mm o.d.) on a FT

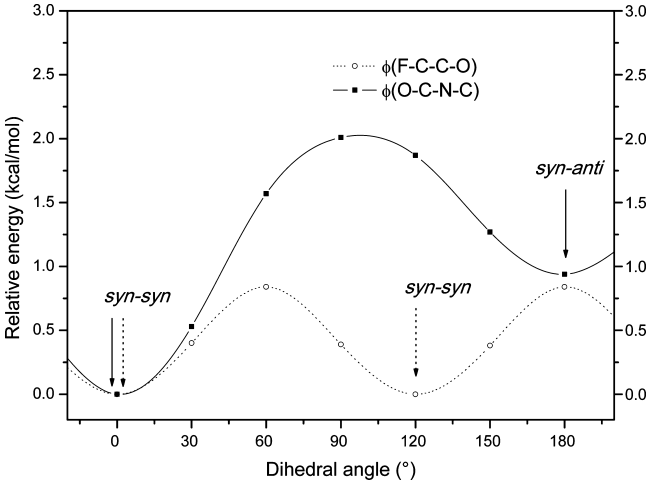

Figure 2. Potential energy curve of $CF_3C(O)NCS$ for rotation along C−C and C−N bonds calculated at B3LYP/6-311+(d) level of approximation.

Table 1. Energy Differences (kcal mol^{-1}) between syn−syn and syn−anti Forms and Transition State (TS) of $CH_3C(O)NCS$ and $CF_3C(O)NCS$ Computed Using Different Levels of Approximation Relative to the Most Stable syn−syn Conformer

model	$\Delta E°$	$\Delta H°$	$\Delta G°$	$\Delta E°$ (TS)	$E_{a_{syn\text{-}anti\rightarrow syn\text{-}syn}}$
	$CH_3C(O)NCS$				
B3LYP/6-311++G(d,p)	1.23[a]	1.25	1.06	1.63	0.40
B3LYP/6-311++G(3df,3pd)	0.76	0.77	0.68	1.36	0.59
MP2/6-311++G(d,p)	0.56	0.54	0.34	1.68	1.12
MP2/6-311+G(3df,2p)	0.07[b]				
G2(MP2,SVP)	0.36[b]				
QCISD(T)/6-31G*	1.34[b]				
B3PW91/6-311+G(d)	1.25[a]				
	$CF_3C(O)NCS$				
B3LYP/6-311++G(d,p)	0.88	0.87	0.86	1.84	0.96
B3LYP/6-311++G(3df,3pd)	0.50	0.48	0.51	1.70	1.20
MP2/6-311++G(d,p)	0.17	0.13	0.35	2.12	1.95

[a]Reference 23. [b]Reference 24.

dx.doi.org/10.1021/jp4110085 | J. Phys. Chem. A 2014, 118, 697−707

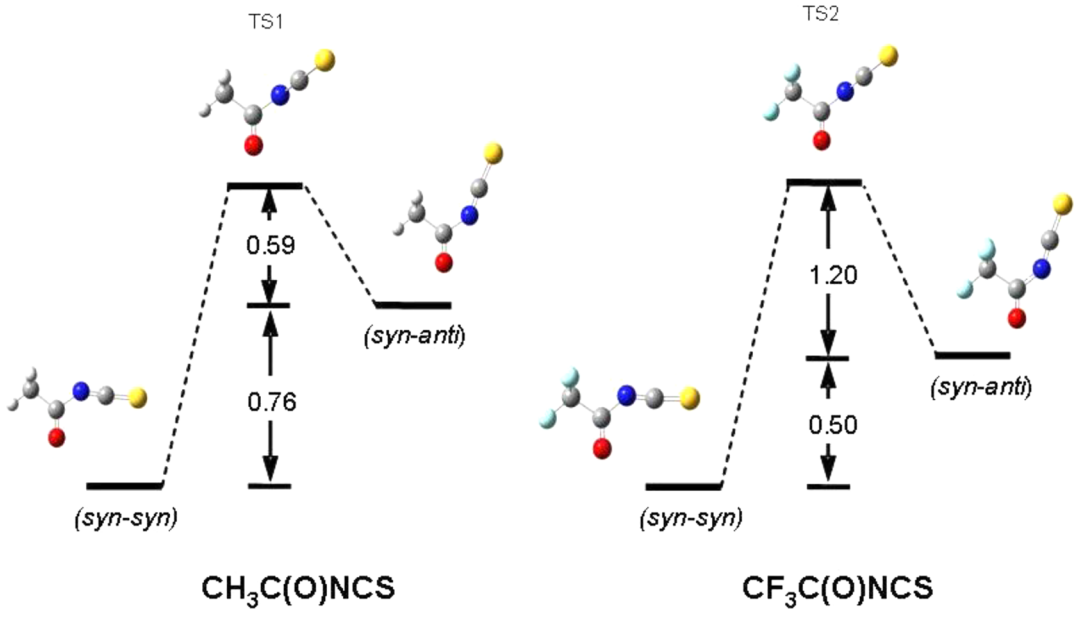

Figure 3. Optimized structures, relative energies ($\Delta E°$), and transition states (TS) for $CH_3C(O)NCS$ and $CF_3C(O)NCS$ calculated with the B3LYP/6-311++G(3df,3pdf) method.

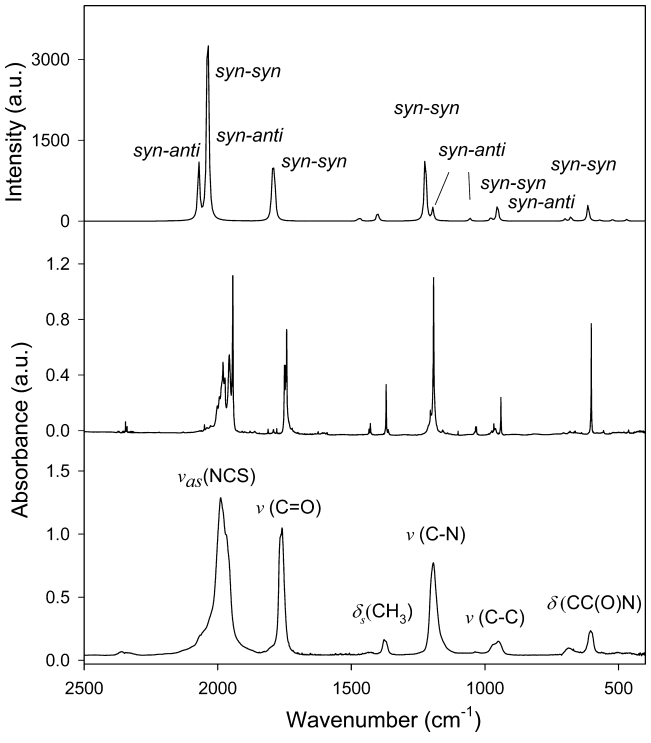

Figure 4. Upper trace: Computed IR spectrum of $CH_3C(O)NCS$ for a conformer composition of 76% syn−syn and 24% syn−anti using the B3LYP/6-311++G(3df,3pd) approximation. The spectral bands were simulated using Lorentzian forms with a bandwidth of 5 cm^{-1}. The intensity is given in km mol^{-1}. Middle trace: IR spectrum of $CH_3C(O)NCS$ isolated in an Ar matrix (1:1000) at 15 K (resolution: 0.5 cm^{-1}). Lower trace: IR spectrum of gaseous $CH_3C(O)NCS$ at 298 K (resolution: 2 cm^{-1}).

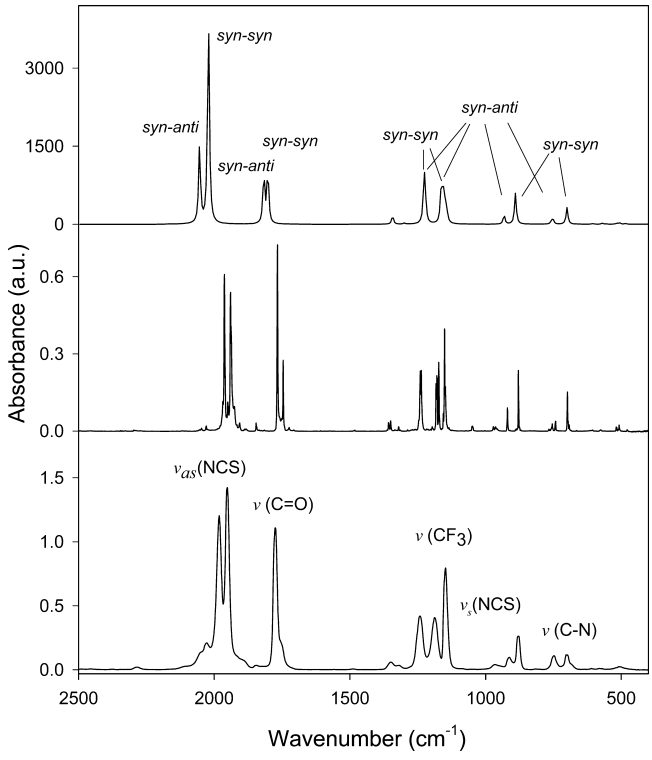

Figure 5. Upper trace: Computed IR spectrum of $CF_3C(O)NCS$ for a conformer composition of 70% syn−syn and 30% syn−anti using the B3LYP/6-311++G(3df,3pd) approximation. The spectral bands present Lorentzian forms with a bandwidth of 5 cm^{-1}. The intensity is given in km mol^{-1}. Middle trace: IR spectrum of $CF_3C(O)NCS$ isolated in an Ar matrix (1:1000) at 15 K (resolution: 0.25 cm^{-1}). Lower trace: IR spectrum of gaseous $CF_3C(O)NCS$ at 298 K (resolution, 2 cm^{-1}).

Bruker RFS 106/S spectrometer, equipped with a 1064 nm Nd:YAG laser, in the region from 4000 to 100 cm^{-1} using a resolution of 2 cm^{-1}.

(c). Matrix Isolation Experiments. Experiments on $CH_3C(O)NCS$ were performed in La Plata using a gas mixture of the sample in argon (1:1000) in a 1 L glass storage container. The mixture was deposited on a CsI window cooled at 15 K by means of a Displex closed-cycle refrigerator using the pulse deposition technique. IR spectra of each matrix sample were

dx.doi.org/10.1021/jp4110085 | J. Phys. Chem. A 2014, 118, 697−707

Table 2. Experimental and Theoretical Wavenumbers (cm^{-1}) and Assignments of the Normal Modes of Vibration of $CH_3C(O)NCS$

Mode	Experimental IR gas[a],[b]	Experimental IR gas[c],[b]	Experimental Ar matrix[d]		Computed[e] *syn-syn*	Computed[e] *syn-anti*	Assignment[c],[f] / Symmetry
ν_1	3032 (vw)	-	3027.5	(<1)	3159 (8)	3156 (5)	$\nu_{as}(CH_3)$ / A'
ν_2	-	-	2966.5	(<1)	3102 (2)	3104 (3)	$\nu_{as}(CH_3)$ / A''
ν_3	-	2935 (w)	2935.9	(<1)	3046 (1)	3045 (1)	$\nu_s(CH_3)$ / A'
	2665 (w)	-	2658.9 2635.2	(1)			2 ν_8 or $\nu_5 + \nu_{12}$
ν_4	1989 (vs) 1967 (sh)	1990 (vs) 1968 (sh)	1974.3 1980.0 1956.9 1943.7*	(100)	2037 (1650)	2071 (1344)	ν_{as}(NCS) / A'
ν_5	1762 (s)	1763 (s)	1751.7 1750.4 1745.9 1741.9*	(28)	1788 (340)	1795 (922)	ν(C=O) / A'
ν_6	-	-	-		1474 (9)	1478 (10)	$\delta_{as}(CH_3)$ / A''
ν_7	1433 (w)	1430 (vw)	1433.6 1428.9*	(1)	1467 (16)	1468 (7)	$\delta_{as}(CH_3)$ / A'
ν_8	1374 (m)	1373 (m)	1369.4 1362.2	(5)	1402 (61)	1395 (23)	$\delta_s(CH_3)$ / A'
ν_9	1193 (s)	1193 (s)	1204.2 1192.1* 1154.8	(32)	1223 (516)	1195 (282)	ν(C-N) / A'
ν_{10}	-	1092 (vw)	-		1057 (6)	1057 (6)	$\rho(CH_3)$ / A''
ν_{11}	1032 (vw)	1037 (vw)	1034.8 1031.6	(1)	1055 (13)	1033 (1)	$\rho(CH_3)$ / A'
ν_{12}	958 (m)	-	975.1 966.8 940.2*	(7)	953 (124)	978 (74)	ν(C-C) / A'
ν_{13}	685 (w)	696 (w)	681.8	(<1)	678 (32)	700 (52)	ν_s(NCS) / A'
ν_{14}	604 (m)	600 (m)	601.8	(7)	614 (125)	523 (35)	δ(CC(O)N) / A'
ν_{15}	564 (vw)	570 (w)	556.1	(<1)	570 (6)	573 (6)	δ(CC(O)N) / A''
ν_{16}	503 (vw)	510 (w)			494 (<1)	489 (<1)	δ(NCS) / A''
ν_{17}		450 (w)			468 (7)	471 (19)	δ(NCS) / A'
ν_{18}					358 (7)	404 (<1)	δ(CCN) / A'
ν_{19}					119 (<1)	128 (<1)	$\tau(CH_3)$ / A''
ν_{20}					87 (1)	83 (6)	δ(CNC) / A''
ν_{21}					65 (1)	56 (1)	τ(NCS) / A''

[a]This work. [b]Band intensity: vs, very strong; s, strong; m, medium; w, weak; vw, very weak; sh, shoulder. [c]Reference 27. [d]Relative intensities between parentheses. *The more intense matrix band of the presumable more stable trapping site. [e]Wavenumbers (cm^{-1}) and intensities between parentheses (km mol^{-1}) computed with the B3LYP/6-311+G(3df) model. [f]ν, δ, ρ, τ and oop represent stretching, deformation, rocking, torsion and out-of-plane modes, respectively.

recorded with a Nexus Nicolet instrument at a resolution of 0.5 and 0.125 cm^{-1} with 64 scans using MCTB and DTGS detector for the ranges 4000−400 or 600−180 cm^{-1}, respectively. For photolysis experiments, the matrix was exposed to a broad-band UV−vis radiation ($200 \leq \lambda \leq 800$ nm) from a Hg−Xe arc lamp operating at 1000 W, using a water filter in the output to absorb IR radiation and to minimize any heating effects.

For matrix isolation experiments carried out in Wuppertal, $CF_3C(O)NCS$ was diluted with argon in a ratio of 1:1000 in a 1 L stainless-steel storage container, and then small amounts of the mixture were deposited within 10 min onto the cold matrix support (16 K, Rh-plated Cu-block) in a high vacuum (10^{-5} Pa). Temperature-dependent conformational studies were carried out by passing the gaseous sample/Ar mixtures through a quartz nozzle (1 mm i.d.), heated over a length of ~10 mm with a platinum wire (0.25 mm o.d.) prior to deposition on the matrix support. The nozzle was held at 298 or 723 K.

IR spectra of matrix-isolated samples were recorded in a reflectance mode on a Bruker IFS 66v/S spectrometer using a transfer optic. A liquid N_2 cooled HgCdTe detector (MCT) and a KBr/Ge beam splitter were used in the wavenumber range 5000 to 530 cm^{-1}. For each spectrum with an apodized resolution of 0.25 cm^{-1} 200 scans were added. More details of the matrix apparatus are given elsewhere.[19]

(d). UV Spectroscopy. The UV−vis spectrum of gaseous $CH_3C(O)NCS$ was recorded using a glass cell equipped with quartz windows (10 cm optical path length) on a Lambda EZ210 UV/vis spectrometer (Perkin-Elmer). Measurements were carried out in the spectral region from 190 to 700 nm with a sampling interval of 1.0 nm, a scan speed of 200 nm min^{-1}, and a slit of 2 nm. The UV−vis spectrum of gaseous $CH_3C(O)NCS$

dx.doi.org/10.1021/jp4110085 | J. Phys. Chem. A 2014, 118, 697−707

Table 3. Experimental and Theoretical Wavenumbers (cm^{-1}) and Assignments of the Normal Modes of Vibration of $CF_3C(O)NCS$

	experimental						
	IR				computed[e]		
mode	gas[a,b]	gas[c,b]	matrix Ar[d]		syn−syn	syn−anti	assignment[c,f]/symmetry
ν_1	1982 vs	1982 vs	1962.7	(77)		2054 (1443)	ν_{as}(NCS)/A′
	1952 vs	1952 vs	1940.3	(100)	2021 (1674)		
ν_2	1775 vs	1775 vs	1767	(62)		1817 (944)	ν(C═O)/A′
	1753 sh	1753 sh	1745.9	(22)	1803 (425)		
ν_3	1350 w	1352 w	1350	(3)	1343 (67)		ν(C−C)/A′
	1321 sh	1325 w	1320.3	(1)		1300 (18)	
ν_4	1242 m	1243 m	1240.6	(41)	1227 (387)		$\nu_{as}(CF_3)$/A′
			1236.9			1222 (273)	
ν_5	1187 m	1187 m	1182.3/1179.2	(22)	1163 (268)		$\nu_s(CF_3)$/A′
			1172.5	(17)		1161 (140)	
ν_6	1148 s	1148 s	1151.2	(40)	1153 (264)		$\nu_{as}(CF_3)$/A″
			1148			1143 (250)	
	967 vw	966 w	963	(4)			
ν_7	912 w	912 w	919.4	(6)		932 (169)	ν_s(NCS)/A′
	880 m	883 m	879	(13)	890 (246)		
ν_8	748 w	764 sh	754.3	(3)	757 (18)		ν(C−N)/A′
			752.5			751 (34)	
ν_9	748 w	748 w	743.4	(3)		751 (19)	δ(CC(O)N)/A″
			741.8		753 (17)		
ν_{10}	700 w	701 w	698.3	(11)	700 (132)		$\delta_s(CF_3)$/A′
	579 vw		573.7	sh		556 (5)	
ν_{11}	611 vw	612 vw	605.2	(1)		605 (10)	$\delta_{as}(CF_3)$/A′
	579 vw	540 bd	575.6	(1)	569 (8)		
ν_{12}	518 sh	500 bd	518.2	(1)	518 (6)		$\delta_{as}(CF_3)$/A″
			507.6			512 (6)	
ν_{13}	506 vw		503.3	(2)	496 (<1)	488 (<1)	δ(NCS)/A″
ν_{14}	473 vw	436 bd	478.4	(1)	484 (6)	505 (24)	δ(NCS)/A′
ν_{15}					406 (6)	391 (<1)	δ(CC(O)N)/A′
ν_{16}		336 m				368 (<1)	$\rho(CF_3)$/A′
		241 w			334 (4)		
ν_{17}		246			247 (4)	247 (4)	$\rho(CF_3)$/A″
ν_{18}					209 (<1)	241 (7)	δ(CCN)/A′
ν_{19}		55 w			71 (1)	61 (<1)	δ(CNC)/A′
ν_{20}		74 w, sh				84 (1)	τ(NCS)/A″
		65 w			67 (<1)		
ν_{21}					29 (1)	23 (<1)	$\tau(CH_3)$/A″

[a]This work. [b]Band intensity: vs, very strong; s, strong; m, medium; w, weak; vw, very weak; sh, shoulder, bd broad. [c]Reference 28. [d]Relative intensities between parentheses. [*]The more intense matrix band of the presumable more stable trapping site. [e]Wavenumbers (cm^{-1}) and intensities between parentheses (km mol^{-1}) computed with the B3LYP/6-311+G(3df) model. [f]ν, δ, ρ, τ, and oop represent stretching, deformation, rocking, torsion and out-of-plane modes, respectively.

shows an absorption band at λ_{max} = 264 nm attributed to the n→π* transition located on the NCS chromophore and a stronger absorption at λ_{max} = 204 nm, which could be due to the π→π* transition in the C═O chromophore, according to reported values for similar molecules.[1,2] The same arguments can be used to assign the UV bands of gaseous $CF_3C(O)NCS$ at 274 and 197 nm.

(e). Quantum Chemical Calculations. Density functional theory (DFT) calculations were performed using the program package GAUSSIAN 03.[20] MP2 calculations[21] were carried out with the Firefly program.[22] In the first step, the potential curve of internal rotations along the XC−CO (X = H, F) and OC−NC dihedral angles were calculated at the B3LYP/6-311++(dp) and B3LYP/6-311+(d) level of approximations for $CH_3C(O)$-NCS and $CF_3C(O)NCS$, respectively, by optimizing the molecular geometry with fixed torsion angles in the range from 0 to 180 and step size of 30° (see Figures 1 and 2). The optimized structures, the relative energies, and the rotational transition states for both derived forms computed with the B3LYP/6-311++G(3df,3pdf) level of approximation are depicted together in Figure 3.

In this way, two low energy conformations were found for each molecule: syn−syn and syn−anti. Using several approximations listed in Table 1 full geometry optimizations of these conformers were performed. Subsequent calculations of vibrational frequencies proved that they correspond to true minima on the potential energy surface.

RESULTS AND DISCUSSION

Quantum Chemical Calculations. To evaluate the conformational equilibrium of $CH_3C(O)NCS$ and $CF_3C(O)NCS$, the potential energy curves for the internal rotation around the C−N single bonds for both molecules were computed by

dx.doi.org/10.1021/jp4110085 | J. Phys. Chem. A 2014, 118, 697−707

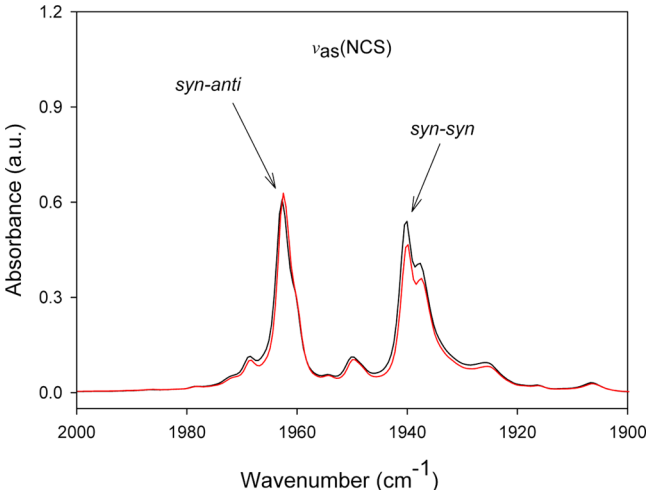

Figure 6. IR spectra of $CF_3C(O)NCS$ in the 2000−1900 cm^{-1} region corresponding to the antisymmetric NCS normal mode of vibration with nozzle temperatures at 25 °C (black line) and 450 °C (red line) isolated in an Ar matrix (1:1000) at 15 K (resolution: 0.25 cm^{-1}).

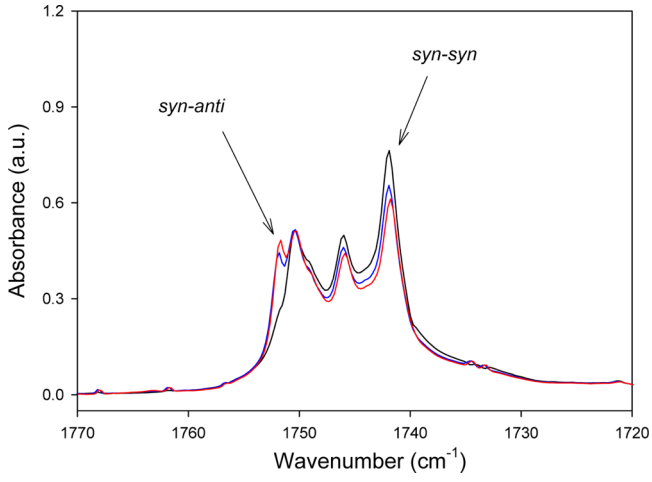

Figure 8. Randomization process occurring in an Ar matrix of $CH_3C(O)NCS$ after 1 and 2 min of broad band UV−vis light ($200 \leq \lambda \leq 800$ nm) irradiation. The black, blue, and red lines indicate matrix without and after 1 and 2 min irradiation, respectively.

structure optimization at fixed dihedral angles ϕ(OC−NC) from 0° to 180° in steps of 30° as is shown in Figures 1 and 2. The derived molecular structures of syn−syn and syn−anti forms were fully optimized at different levels of approximation to verify that they correspond to minimum energy structures and to provide zero-point vibrational energy corrections. Computed relative energies between syn−syn and syn−anti forms and transition states (TS) of $CH_3C(O)NCS$ and $CF_3C(O)NCS$ computed using different levels of approximation relative to the most stable syn−syn conformer are listed in Table 1.

Moreover, optimized structures for the syn−syn and syn−anti rotamers of $CH_3C(O)NCS$ and $CF_3C(O)NCS$ together with their rotational transition states and the $\Delta E°$ relative energies calculated with the method B3LYP/6-311++G-(3df,3pdf) are depicted in Figure 3.

For $CH_3C(O)NCS$ the syn−syn form is predicted to be lower in energy ($\Delta E°$) by 1.2/0.1 kcal mol^{-1} with respect to the syn−anti rotamer. For $CF_3C(O)NCS$ the syn−syn rotamer is also predicted to be the most stable by 0.9/0.2 kcal mol^{-1}.

The preference of the syn−syn form in both molecules can probably be explained in terms of the mesomeric (resonance) and anomeric effects.[25] In particular, for this conformer a mayor

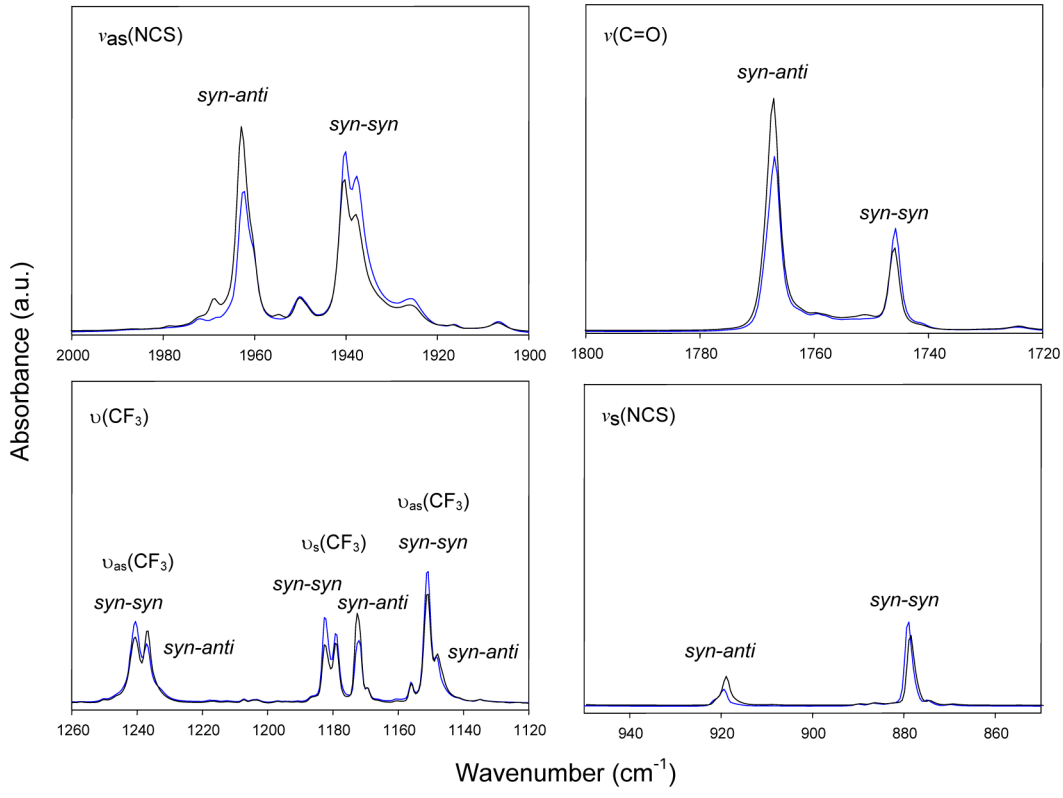

Figure 7. Ar-matrix IR spectra of $CF_3C(O)NCS$ before (black) and after annealing (blue) the matrix to 30 K for a matrix deposited at 450 °C.

dx.doi.org/10.1021/jp4110085 | J. Phys. Chem. A 2014, 118, 697−707

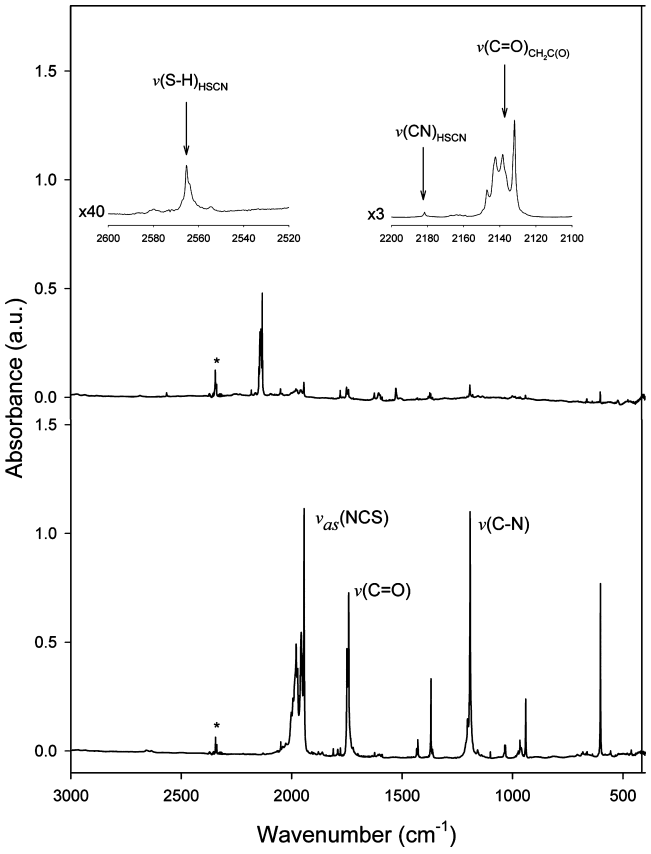

Figure 9. IR spectra of an Ar matrix containing $CH_3C(O)NCS$. Lower trace, following deposition; upper trace, after 60 min of broad-band UV–vis photolysis. Amplified regions between 2600 and 2520 and 2200–2100 cm^{-1} are also included. * denotes an impurity.

energy stabilization is expected through donation of electron density of the σ-type lone-pair on the nitrogen atom into the antibonding orbital of the C=O bond, $lp_\sigma(N) \rightarrow \sigma^*(C{=}O)$, according to the anomeric effect. In contrast, the major stability of the anti conformer in ClC(O)NCS is intriguing and calculations suggest that the $lp_\sigma(N) \rightarrow \sigma^*(C{-}Cl)$ delocalization is predominant in the isothiocyanate moiety.[26]

An interesting result that follows from the potential energy curves for $CH_3C(O)NCS$ and $CF_3C(O)NCS$ (Figures 1 and 2) is their very small rotational barrier value. Computed energy barriers E_a for the syn–anti → syn–syn internal rotation of $CH_3C(O)NCS$ and $CF_3C(O)NCS$ derived from fully optimized transition state structures at various levels of theory are listed in Table 1. The transition state structures (Figure 3) were verified by an intrinsic reaction coordinate calculation to connect the conformers along the reaction path for the normal coordinate of the imaginary frequency. Values lower than 2 kcal mol^{-1} were computed for all cases, which agree with experimental results discussed below.

Matrix Isolation Experiments. The syn–anti/syn–syn conformational equilibrium of both $CH_3C(O)NCS$ and $CF_3C(O)NCS$ in the gas phase, reproduced by quantum chemical calculations, is consistent with IR spectra recorded in the gas phase and in solid Ar (Figures 4 and 5). However, more experimental information is desirable to characterize the conformational properties and the photochemical behavior of these compounds. The vibrational data are collected in Table 2 for $CH_3C(O)NCS$ whereas Table 3 lists vibrational data corresponding to $CF_3C(O)NCS$ in correspondence with results of Figure 5.

The matrix isolation technique could be used to estimate the enthalpy energy difference, ΔH°_{exp}, between stable conformers from IR spectra of mixtures deposited at different nozzle temperatures. However, for both molecules with OC–NC rotational barriers lower than ~3 kcal mol^{-1} between the rotamers, a disturbance of the gas-phase equilibrium composition during the deposition at about 15 K has been observed. This behavior has been reported in relevant antecedents of the literature.[29]

However, temperature-dependent Ar-matrix IR spectra were found to be useful to assign vibrational absorptions for both rotamers in the case of $CF_3C(O)NCS$. Ar-matrix IR spectra of this sample obtained for two different nozzle temperatures at 25 and 450 °C are shown in Figure 6.

$CF_3C(O)NCS$ exhibits two absorptions for each vibrational mode due to the syn–anti/syn–syn conformational equilibrium observed in the gas phase (see Figure 6 and Table 3). At the higher nozzle temperature used in the experiments, the IR intensities of the bands at 1962.7, 1767.0, 1236.9, 1172.5, 1148.0, and 919.4 cm^{-1} increase their intensity at the expense of the corresponding bands of the syn–syn $CF_3C(O)NCS$, and they are assigned to stretching modes of the higher energy syn–anti conformer (Table 3). The bands of the most stable form (syn–syn) split due to two different matrix environments.

The small rotational barrier of $CF_3C(O)NCS$ was evaluated by annealing experiments, as was recently reported for the halogenated derivatives FC(O)NCS and ClC(O)NCS, which also exhibit a remarkable very low rotational barrier around the C–N single bond.[30,26] The Ar-matrix IR spectra of $CF_3C(O)$-NCS before and after annealing the matrix to 30 K for a matrix deposited at 450 °C are shown in Figure 7.

Interestingly, the bands assigned to the lower energy syn–syn conformer increase their intensity at expense of the higher energy syn–anti rotamer, which is consistent with the computed small energy barrier for the syn–anti → syn–syn interconversion. In addition, the intensity of the bands attributed to the syn–syn form in two different matrix sites behaved differently, which allowed them to be distinguished. A similar behavior was also observed in the syn → anti interconversion process of anti-ClC(O)NCS isolated in solid rare gases, where it was demonstrated that different solid hosts and the local environment can influence strongly the conversion rate constants.[26]

Photochemistry. Exposure of an Ar matrix doped with roughly 0.1% $CH_3C(O)NCS$ or $CF_3C(O)NCS$ to broad-band UV–vis light ($200 \leq \lambda \leq 800$ nm) resulted in the decay of the bands due to $CH_3C(O)NCS$ or $CF_3C(O)NCS$ and the appearance and growth of new bands belonging to several different photospecies.

$CH_3C(O)NCS$. Figure 8 illustrates FTIR spectra of an Ar matrix of $CH_3C(O)NCS$ after broad-band irradiation for 1 and 2 min and the spectrum recorded immediately after deposition in the 1770–1720 cm^{-1} region, revealing the changes that develop as a result of the randomization implying a diminution in the concentration of the more stable syn–syn and the growth of the syn–anti form.

Figure 9 depicts FTIR spectra of $CH_3C(O)NCS$ of an Ar matrix after broad-band irradiation for 60 min and the spectrum recorded immediately after deposition in the 3000–400 cm^{-1} range and Table 4 lists the corresponding wavenumbers, intensities, and assignments of the IR absorptions. To distinguish the bands corresponding to the different species

dx.doi.org/10.1021/jp4110085 | J. Phys. Chem. A 2014, 118, 697–707

Table 4. Wavenumbers, Intensities, and Assignments of the IR Absorptions Appearing after 60 min Broad-Band UV−vis Photolysis of $CH_3C(O)NCS$ Isolated in an Ar Matrix

IR (matrix Ar)		assignment		
ν (cm^{-1})	I^a	molecule	vibrational mode	wavenumbers reported previously
3498.7	0.001	$H_2C{=}C{=}O$	$\nu(C{=}O) + \delta(CH_2)$	3513[b]
3259.2		$H_2C{=}C{=}O$	$\nu(C{=}O) + \nu(C{-}C)$	3225[b]
3242.0				
3220.4				
3150.2	0.021	$H_2C{=}C{=}O$	$\nu(CH_2)$	3155[b]
3060.0	0.036	$H_2C{=}C{=}O$	$\nu_{as}(CH_2)$	3062[b]
3056.1				
3052.2[d]				
2685.2	0.022			
2565.3	0.015	HSCN	$\nu(S{-}H)$	2581.0[c]
2181.6	0.013	HSCN	$\nu(C{\equiv}N)$	2182.3[c]
2166.9	0.015	$H_2C{=}C{=}O$	$\nu(C{=}O)$	
2163.9				
2161.9				
2158.9				
2147.1	1.000	$H_2C{=}C{=}O$	$\nu(C{=}O)$	2142[b]
2143.9				
2142.3				
2138.4				
2131.9[d]				
2095.7	0.010	$H_2C{=}C{=}O$	$\nu(^{13}C{=}O)$	2085[b]
2091.4				
2085.8				
1381.0	0.002	$H_2C{=}C{=}O$	$\delta(CH_2)$	1381[b]
972.0	0.001	$H_2C{=}C{=}O$	$\rho(CH_2)$	974[b]
964.5	0.002	HSCN	δ(HSC)	959.7[c]
521.9	0.040	$H_2C{=}C{=}O$	oop. (C=O)	525[b]

[a]Relative intensity. [b]Reference 31. [c]Reference 32. [d]Impurity.

and help determine the sequence of the changes, the integrated intensities of the new bands have been plotted as a function of irradiation time, as depicted in Figure 10 for an Ar matrix. One family of absorptions of which the most intense occurs at 2147.1 cm^{-1} and is accompanied by much weaker features at 3498.9, 3150.2, 3060.0, 1381.0, and 521.9 cm^{-1} grows continuously with photolysis. This is readily identifiable with the formation of H_2CCO. Other absorptions occurring near 2564.4 and 2181.6 cm^{-1} grow together during the first hour and then decay somewhat. On the basis of earlier studies, these can be assigned to the molecule of HSCN. During this photochemical process the generation of the thermodynamically less stable HSCN instead of the more stable form HNCS is observed.[32] Differences with the reported wavenumbers for HSCN are attributed to the presence of H_2CCO in the same matrix cage originating interactions or molecular complexes. This second option would be supported with the displacement at 2147.1 cm^{-1} evidenced by the ketene.[31]

According to these evidence the main photochemical channel can be schematically described as in Figure 11.

Thus, after the photoexcitation process the molecule changes its form reaching one of its many available excited states. One of the events involving the C=O carbonylic chromophore would lead to the lost of planarity in the molecular geometry inducing a pyramidal structure around the carbonylic carbon. From such an excited state, the molecule should create radicals to form the end products of the Figure 11. If the C−N bond is broken, one H atom would roam or migrate inside the matrix cage from the methyl fragment to the opposite molecular extreme, the S atom, to give the thiocyanic acid, HSCN.[33]

Table 5. Wavenumbers, Intensities, and Assignments of the IR Absorptions Appearing after 33 min Broad-Band UV−vis Photolysis of $CF_3C(O)NCS$ Isolated in an Ar Matrix

IR (Matrix Ar)		assignment		
ν (cm^{-1})	I^a	molecule	vibrational mode	wavenumbers reported previously
2138.6	0.333	C≡O	$\nu(C{\equiv}O)$	2139[b]
2134.0[e]				
1998.5	0.509	CF_3NCS	ν_{as}(NCS)	2005[c]
1987.5				2055 (1389)[d]
1265.0	0.569	CF_3NCS	$\nu(C{-}N)$	1265[c]
1261.9				1267 (760)[d]
1232.4	0.269			
1228.5				
1204.9	1.000	CF_3NCS	$\nu_{as}(CF_3)$/A′	1205[c]
1198.1[e]				1171 (357)[d]
1190.6				
1186.9				
1109.5	0.133	CF_3NCS	$\nu_{as}(CF_3)$/A′	1134 (388)[d]
1106.5				
988.4	0.142	CF_3NCS	$\nu_s(CF_3)$	986[c],982[c]
				984 (291)[d]
650.6	0.058	CF_3NCS	$\delta_{as}(CF_3)$/A′	655[c],650[c]
				641 (51)[d]
621.6	0.010	CF_3NCS	$\delta_{as}(CF_3)$/A″	593 (3)[d]
554.1	0.005	CF_3NCS	$\delta_s(CF_3)$/A′	543 (1)[d]

[a]Relative intensity. [b]Reference 34. [c]References 35 and 36. [d]Computed with the B3LYP/6-311+G(3df) approximation. Intensities between parentheses (km mol^{-1}). [e]Impurity.

dx.doi.org/10.1021/jp4110085 | J. Phys. Chem. A 2014, 118, 697−707

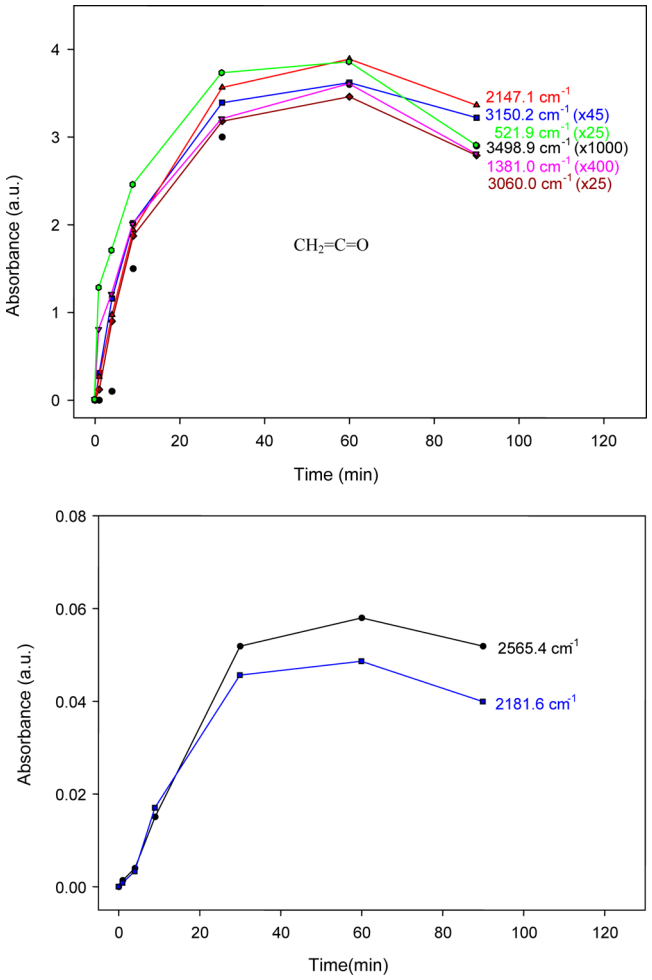

Figure 10. Plots as a function of irradiation time of the intensities of the bands of H_2CCO (upper panel) and HSCN (lower panel) assigned in the IR spectrum of an Ar matrix initially containing $CH_3C(O)NCS$.

$CF_3C(O)NCS$. The formal change of H by F atoms in the $CH_3C(O)NCS$ molecule has dramatic consequences in the photochemical processes of $CF_3C(O)NCS$. Figure 12 shows the IR spectra before and after irradiation and Table 5 collects the corresponding wavenumbers, intensities, and assignments of the IR absorptions.

The isolation, identification, and characterization of trifluoromethyl isothiocyanate, CF_3NCS, have been achieved through photodecomposition of the parent molecule following the elimination of CO. The experimental wavenumbers prove to be in excellent agreement with the results of the computations (see Table 5). The family of absorptions of which the most intense occurs near 1200 cm^{-1} and is accompanied by weaker features near 2000, 1265, 1110, and 990 cm^{-1} and much weaker bands near 650, 620, and 555 cm^{-1} grows continuously with

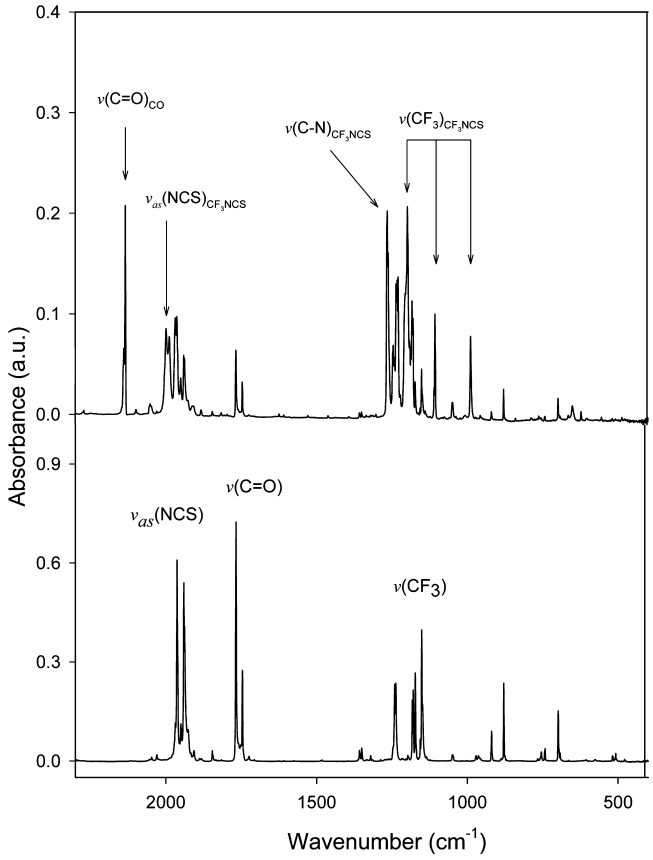

Figure 12. IR spectra of an Ar matrix containing $CF_3C(O)NCS$. Lower trace, following deposition; upper trace, after 33 min of broad-band UV–vis photolysis.

photolysis. This is readily identifiable with the formation of only one species, namely, CF_3NCS.

CONCLUSION

The vapors of $CH_3C(O)NCS$ and $CF_3C(O)NCS$ have been shown by experiment and theory to consist of an equilibrium mixture of syn–syn and syn–anti conformers.

Broad-band UV–vis irradiation of the matrix-isolated compounds results in the following changes: (i) interconversion of the syn–syn and syn–anti conformers in a randomization process tending to lead to a roughly equimolar mixture of the two forms in both molecules (ii) both forms of $CH_3C(O)NCS$ and $CF_3C(O)NCS$ suffer photodecomposition which appears to follow two distinct reaction channels, $CH_3C(O)NCS$ leading to HSCN and H_2CCO, and $CF_3C(O)$-NCS forming CO and CF_3NCS. A DFT method has been used to estimate wavenumbers of the CF_3NCS molecule.

Any attempt to give a mechanistic interpretation of the various changes must take into account the following aspects. (i) The photolysis conditions were relatively unselective, the

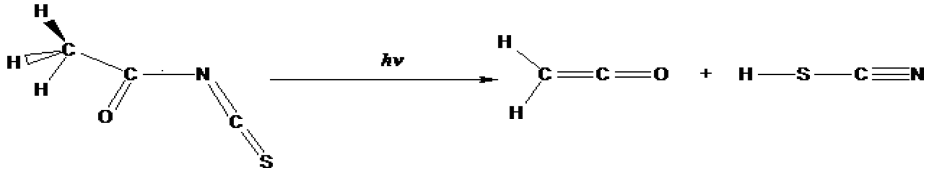

Figure 11. Schematic representation of the main photoevolution channel of $CH_3C(O)NCS$ isolated in an Ar matrix at 15 K after broad-band UV–vis photolysis.

dx.doi.org/10.1021/jp4110085 | J. Phys. Chem. A 2014, 118, 697–707

radiation spanning the wavelength range 200−800 nm, and the involvement of photolabile products, as well as the photolabile precursor, makes it impossible to judge the nature of the photoactive transitions with any certainty. Attempts to restrict more closely the wavelength range served only to retard the changes to an unacceptable extent. (ii) The matrix cage effect may be expected to inhibit the separation of molecular and even atomic products following photodissociation. In regard to $CH_3C(O)NCS$ ketene, H_2CCO, is formed as a stable final photoproduct. The remaining H atom of the molecule roams or migrates inside the matrix cage to form with the remaining NCS fragment the thiocyanic acid and not the isothiocyanic acid. It is remarkable because the thermodynamic more stable isomer is HNCS. In the case of $CF_3C(O)NCS$, the photoevolution process changes considerably being the stable CO molecule and CF_3NCS the main matrix photoevolution products.

AUTHOR INFORMATION

Corresponding Author

*E-mail: carlosdv@quimica.unlp.edu.ar. Tel: 0054 221 4259485.

Notes

The authors declare no competing financial interest.

ACKNOWLEDGMENTS

The Argentinean authors thank the Agencia Nacional de Promoción Científica y Técnica (ANPCYT), Consejo Nacional de Investigaciones Científicas y Técnicas (CONICET), Facultad de Ciencias Exactas, Universidad Nacional de La Plata (UNLP). L.A.R. gratefully acknowledges the DAAD, UNLP, and Bergische Universität Wuppertal. C.O.D.V. acknowledges the DAAD, which generously sponsored the DAAD Regional Program of Chemistry for the Argentina supporting Latin-American students to do their Ph.D. in La Plata. C.O.D.V., H. B., and H. W. acknowledge the support from the Deutsche Forschungsgemeinschaft and the Fonds der Chemischen Industrie.

REFERENCES

(1) Ramos, L. A.; Ulic, S. E.; Romano, R. M.; Vishnevskiy, Yu. V.; Mitzel, N. W.; Beckers, H.; Willner, H.; Tong, S.; Ge, M. F.; Della Védova, C. O. Chlorodifluoroacetyl Isothiocyanate, $ClF_2CC(O)NCS$: Preparation, Structural and Spectroscopic Studies. *J. Phys. Chem. A.* **2013**, *117*, 5597−5606.

(2) Ramos, L. A.; Ulic, S. E.; Romano, R. M.; Tong, S.; Ge, M. F.; Vishnevskiy, Yu. V.; Berger, R. J. F.; Mitzel, N. W.; Beckers, H.; Willner, H.; Della Védova, C. O. Chlorodifluoroacetyl Cyanide, $ClF_2CC(O)CN$: Synthesis, Structure, and Spectroscopic Characterization. *Inorg. Chem.* **2011**, *50*, 9650−9659.

(3) Koch, R.; Wentrup, C. Rearrangements of Acyl, Thioacyl, and Imidoyl (Thio)cyanates to Iso(thio)cyanates, Acyl Iso(thio)cyanates to (Thio)acyl Isocyanates, and Imidoyl Iso(thio)cyanates to (Thio)-acyl Carbodiimides, RCX-YCN ⇌RCX-NCY ⇌ RCY-NCX ⇌ RCY-XCN (X and Y = O, S, NR′). *J. Org. Chem.* **2013**, *78* (5), 1802−1810.

(4) Sommerlade, R.; Ekici, P.; Parlar, H. Gas phase reaction of selected isothiocyanates with OH radicals using a smog chamber-mass analyzer system. *Atmos. Environ.* **2006**, *40*, 3306−3315.

(5) Vermeulen, M.; Zwaneburg, B.; Chittenden, G. J. F.; Verhagen, H. Synthesis of isothiocyanate-derived mercapturic acids. *Eur. J. Med. Chem.* **2003**, *38*, 729−737.

(6) Kwang-Hee Park, K. H.; Jeon, J.; Park, Y.; Lee, S.; Park, H.-S.; Han, H.; Cho, Ch. Infrared Probes Based on Nitrile-Derivatized Prolines: Termal Insulation Effect and Enhanced Dynamic Range. *J. Phys. Chem. Lett.* **2013**, *4*, 2105−2110.

(7) Smith, P. A. S.; Emerson, D. W. The Isomerization of Alkyl Thiocyanates to Isothiocyanates. *J. Am. Chem. Soc.* **1960**, *82*, 3076−3082.

(8) Abe, H.; Kawanda, M.; Inoue, H.; Ohba, S.; Nomoto, A.; Watanabe, T.; Shibasaki, M. Syntesis of Intervenolin, an Antitumor Natural Quinolone with Unusual Substitutents. *Org. Lett.* **2013**, *15*, 2124−2127.

(9) Iliceto, A.; Fava, A.; Mazzucato, U.; Rosseto, O. Thiocyanates and Isothiocyanates. III. Kinetics and Mechanism of Benzhydryl Thiocyanates Isomerization. *J. Am. Chem. Soc.* **1961**, *83*, 2729−2734.

(10) Fava, A.; Iliceto, A.; Ceccon, A.; Koch, P. Isomerization and Isotopic Exchange of 4,4′-Dimethylbenzhydryl Thiocyanate in Acetonitrile. Partition of Electron-Deficient Intermediates between Thio- and Isothiocyanate. *J. Am. Chem. Soc.* **1965**, *87*, 1045−1049.

(11) Fava, A.; Ilicet, A.; Bresadola, S. Ambident Reactivity of Thiocyanate Ion. Thiocyanate Ion Catalysis in the Isomerization of Organic Thiocyanates. *J. Am. Chem. Soc.* **1965**, *87*, 4791−4794.

(12) Loos, R.; Kobayashi, S.; Mayr, H. Ambident Reactivity of the Thiocyanate Anion Revisited: Can the Product Ratio Be Explained by the Hard Soft Acid Base Principle? *J. Am. Chem. Soc.* **2003**, *125*, 14126−14132.

(13) Smith, P. A. S.; Emerson, D. W. The Isomerization of Alkyl Thiocyanates to Isothiocyanates. *J. Am. Chem. Soc.* **1960**, *82*, 3076−3082.

(14) Halfen, D. T.; Ziurys, L. M.; Brünken, S.; Gottlieb, C. A.; McCarthy, M. C.; Thaddeus, P. Detection of a new interstellar molecule: Thiocyanic Acid HSCN. *Astrophys. J.* **2009**, *702*, L124−L127.

(15) Frerking, M. A.; Linke, R. A.; Thadeus, P. Interstellar isothiocyanic acid. *Astrophys. J.* **1979**, *234*, L143−L145.

(16) Lahankar, S. A.; Chambreau, S. D.; Townsend, D.; Suits, F.; Farnum, J.; Zhang, X.; Bowman, J. M.; Suits, A. G. The roaming atom pathway in formaldehyde decomposition. *J. Chem. Phys.* **2006**, *125*, 44303−10pg.

(17) Campbell, N. L.; Gillis, C. J.; Klapstein, D.; Nau, W. M.; Balfour, W. J.; Fougere, S. G. Vibrational Spectra and Conformational Behaviour of Carbonyl Isothiocyanates X-CO-NCS, X = F, Cl, Br, MeO, EtO, and Acetyl Isothiocyanate CH_3-CO-NCS. *Spectrochim. Acta* **1994**, *51A*, 787−798.

(18) Gombler, W.; Willner, H. A Method for Opening and Resealing Glass Ampoules Several Times Under Sustained Vacuum. *J. Phys. E: Sci. Instrum.* **1987**, *20*, 1286−1288.

(19) Schnöckel, H. G.; Willner, H. *Infrared and Raman Spectroscopy, Methods and Applications*; VCH: Weinheim, 1994; pp 297−299.

(20) Frisch, M. J.; Trucks, G. W.; Schlegel, H. B.; Scuseria, G. E.; Robb, M. A.; Cheeseman, J. R.; Montgomery Jr., J. A.; Vreven, T.; Kudin, K. N.; Burant, J. C. et al. *Gaussian 03*, revision B.04 ed.; Gaussian, Inc.: Pittsburgh, PA, 2003.

(21) Møller, C.; Plesset, M. S. Note on an Approximation Treatment for Many-Electron Systems. *Phys. Rev.* **1934**, *46*, 618−622.

(22) Granovsky, A. A. *Firefly* version 7.1.G; www http://classic.chem.msu.su/gran/firefly/index.html. Accessed January 11, 2014.

(23) Zeng, X.; Yao, L.; Ge, M. F.; Wang, D. X. Experimental and theoretical studies on the electronic properties of acetyl pseudohalides $CH_3C(O)X$ (X = NCO, NCS, and N_3). *J. Mol. Struct.* **2006**, *789*, 92−99.

(24) Koch, R.; Wentrup, C. The thioacyl isocyanate−acyl isothiocyanate rearrangement. *Perkin Trans. 2* **2000**, 1846−1850.

(25) Kirby, A. J. *The Anomeric Effect and Related Stereoelectronic Effects at Oxygen*; Springer: New York, 1983.

(26) Ramos, L. A.; Ulic, S. E.; Romano, R. M.; Erben, M. F.; Vishnevskiy, Yu. V.; Reuter, Ch. G.; Mitzel, N. W.; Beckers, H.; Willner, H.; Zeng, X.; Bernhardt, E.; Ge, M. F.; Tong, S. R.; Della Védova, C. O. Spectroscopic Characterization and Constitutional and Rotacional Isomerism of ClC(O)SCN and ClC(O)NCS. *J. Phys. Chem. A.* **2013**, *117*, 2383−2399.

(27) Durig, J. R.; Giurgis, G. A.; Krutules, K. A. Raman and infrared spectra, conformational stability, and ab initio calculations of acetyl isothiocyanate. *J. Mol. Struct.* **1994**, *328*, 97−114.

(28) Durig, J. R.; Giurgis, G. A.; Krutules, K. A. Raman and infrared spectra, conformational stability, barriers to internal rotation and *ab initio* calculations of trifluoroacetyl isothiocyanate. *J. Raman. Spectrosc.* **1995**, *26*, 475−486.
(29) Bodenbinder, M.; Ulic, S. E.; Willner, H. A Gas-Phase and Matriz Isolation Study of the Equilibrium CH_3ONO (Cis) ⇄ CH_3ONO (Trans) by FTIR Spectroscopy. *J. Phys. Chem.* **1994**, *98*, 6441−6444.
(30) Ramos, L. A.; Ulic, S. E.; Romano, R. M.; Erben, M. F.; Lehmann, Ch.L.; Bernhardt, E.; Beckers, H.; Willner, H.; Della Védova, C. O. Vibrational Spectra, Crystal Structures, Constitutional and Rotational Isomerism of FC(O)SCN and FC(O)NCS. *Inorg. Chem.* **2010**, *49*, 11142−11157.
(31) Moore, C. B.; Pimentel, G. C. Infrared Spectrum and Vibrational Potential Function of Ketene and the Deuterated Retenes. *J. Chem. Phys.* **1963**, *38*, 2816−2829.
(32) Wierzejewska, M.; Mielke, Z. Photolysis of isothiocyanic acid HNCS in low- temperature matrices. Infrared detection of HSCN and HSNC isomers. *Chem. Phys. Lett.* **2001**, *349*, 227−234.
(33) Houston, P. L.; Kable, S. H. Photodissociation of acetaldehyde as a second example of the roaming mechanism. *Proc. Natl. Acad. Sci. U.S.A.* **2006**, *103* (44), 16079−16082.
(34) Dubost, H. Infrared absorption spectra of carbon monoxide in rare gas matrices. *Chem. Phys.* **1976**, *12* (2), 139−151.
(35) Fawcett F. S.; Smith W. C. Production of $CF_3C(O)NCS$. U.S. Patent 3174988, 19650323, 1965.
(36) Dahms, G.; Haas, A.; Klug, W. Darstellung und Reaktionen von Fluorthiocarbonylisothiocyanat und Fluorochlorisothiocyanato-methansulfensäurechlorid. *Chem. Ber.* **1971**, *104*, 2732−2742.